REPORT DOCUMENTATION PAGE

Form Approved
OMB No. 0704-0188

1. AGENCY USE ONLY (Leave blank)	2. REPORT DATE	3. REPORT TYPE AND DATES COVERED
	31, July 1997	Technical 6/1/96 - 7/31/96

4. TITLE AND SUBTITLE

New Organic Materials Suitable for Use in Chemical Sensor Arrays

5. FUNDING NUMBERS

N00014-93-11338
300x084yip
96PR0-1027

6. AUTHOR(S)

A.J. Ricco, R.M. Crooks

7. PERFORMING ORGANIZATION NAME(S) AND ADDRESS(ES)

Department of Chemistry
Texas A&M University
College Station, Texas 77843-3255

8. PERFORMING ORGANIZATION REPORT NUMBER

28

9. SPONSORING/MONITORING AGENCY NAME(S) AND ADDRESS(ES)

Office of Naval Research
800 North Quincy Street
Arlington, Virginia 22217-5000

10. SPONSORING/MONITORING AGENCY REPORT NUMBER

11. SUPPLEMENTARY NOTES

Submitted for publication in *Acc. Chem. Res.*

12a. DISTRIBUTION/AVAILABILITY STATEMENT

Reproduction in whole, or in part, is permitted for any purpose of the United States Government. This document has been approved for public release and sale; it's distribution is unlimited.

12b. DISTRIBUTION CODE

13. ABSTRACT *(Maximum 200 words)*

In this paper we discuss several different approaches for preparing chemically sensitive interfaces suitable for array-based chemical sensing applications. The characteristics of all these materials are that they are simple to prepare, synthetically versatile, easy to immobilize on transducer surfaces, exhibit chemical class selectivity to a significant extent, provide rapid (and in most cases fully reversible) responses to analytes, and are relatively durable and inexpensive. The first class of surface coatings are organomercaptan self-assembled monolayers (SAMs) terminated in chemically sensitive functional groups. The second class are bilayers prepared by modifying the aforementioned SAMs with either metal ions or calix[n]arenes. Dendritic polymers confined to surfaces comprise the final class of chemically sensitive interfacial materials. In addition to the synthesis of these materials, we provide *ex-situ* and *in-situ* characterization of their structure and chemical properties as well as their interactions with selected analytes using surface-infrared spectroscopy, surface acoustic wave (SAW) device-based gravimetry, and X-ray photoelectron spectroscopy.

14. SUBJECT TERMS	15. NUMBER OF PAGES
	33
	16. PRICE CODE

17. SECURITY CLASSIFICATION OF REPORT	18. SECURITY CLASSIFICATION OF THIS PAGE	19. SECURITY CLASSIFICATION OF ABSTRACT	20. LIMITATION OF ABSTRACT
Unclassified	Unclassfied	Unclassified	

[Prepared for publication as an Article in *Acc. Chem. Res.*]

New Organic Materials Suitable for Use in Chemical Sensor Arrays

Richard M. Crooks*,[1]

Department of Chemistry

Texas A&M University

College Station, TX 77843-3255

Antonio J. Ricco*,[2]

Microsensor R&D Dept.

Sandia National Laboratories

Albuquerque, New Mexico 87185-1425

[1]E-mail: crooks@chemvx.tamu.edu, Voice: 409-845-5629, Fax: 409-845-1399

[2]E-mail: ajricco@sandia.gov, Voice: 505-844-1405, Fax: 505-844-1198

*Authors to whom correspondence should be addressed

Submitted: 14 August, 1997

Abstract

In this paper we discuss several different approaches for preparing chemically sensitive interfaces suitable for array-based chemical sensing applications. The characteristics of all these materials are that they are simple to prepare, synthetically versatile, easy to immobilize on transducer surfaces, exhibit chemical class selectivity to a significant extent, provide rapid (and in most cases fully reversible) responses to analytes, and are relatively durable and inexpensive. The first class of surface coatings are organomercaptan self-assembled monolayers (SAMs) terminated in chemically sensitive functional groups. The second class are bilayers prepared by modifying the aforementioned SAMs with either metal ions or calix[n]arenes. Dendritic polymers confined to surfaces comprise the final class of chemically sensitive interfacial materials. In addition to the synthesis of these materials, we provide *ex-situ* and *in-situ* characterization of their structure and chemical properties as well as their interactions with selected analytes using surface-infrared spectroscopy, surface acoustic wave (SAW) device-based gravimetry, and X-ray photoelectron spectroscopy.

Introduction

In an accompanying article in this issue,[1] Ricco et al. discuss some of the advantages of using chemical-sensor arrays for many analytical and detection applications. Array-based sensing involves four distinct conceptual steps: development of suitable chemically sensitive interfacial materials, integration of these materials onto suitable sensor platforms, development of pattern-recognition algorithms,[2] and system integration and packaging. In this *Account* we address the first, and arguably the least technologically developed, of these four steps.

There are a number of important factors to consider in developing optimal interfacial materials for integration into chemical sensor arrays: the thickness and structure of the material, the uniqueness of its response to analytes or classes of analytes, ease of synthesis, cost, and durability. The majority of commercially available sensors rely on inorganic materials primarily because of their durability and suitability for operation at elevated temperatures. Inorganic materials will certainly be an important part of next-generation array sensors, but organic materials will play an expanding role because of the vast menu of physical and chemical properties they provide. In particular, organic materials lend themselves to synthetic flexibility, which implies that they can be tailored to exhibit a high level of chemical independence and structural order. The important concept of chemical independence is discussed in another article in this issue.[1] Briefly, however, a material displays chemical independence when it responds to an analyte or class of

analytes in a manner distinct from other materials used in the array. That is, a chemically independent material is one that provides a response that is an analyte-dependent combination of the responses of the other chemically sensitive materials used in the array.[1]

The objectives, then, in designing organic materials for use in chemical sensor-arrays are as follows. First, the materials should be synthetically flexible so that they can be tailored to be chemically independent. Second, they should be cheap and durable. Third, they should be configured on the surface such that they respond quickly to the presence of an analyte. Although this infers the use of thin films such as monolayers, the device usually must function over a large dynamic range of analyte concentrations prior to receptor saturation, which infers thicker polymeric materials. In this *Account*, we describe three new kinds of organic materials that approach these objectives: self-assembled monolayers (SAMs), self-assembled bilayers, and dendrimer monolayers. The focus of the work described here is on the synthesis and characterization of these materials and the development of suitable protocols for their surface immobilization. However, we also report the results of some preliminary experiments aimed specifically at chemical sensing applications.

Experimental Section

Substrates. Au-coated substrates were prepared by electron-beam deposition of 10 nm of Ti or Cr followed by 200 nm of Au onto

Si(100) wafers (Lance Goddard, Assoc., Foster City, CA).[3] Au-coated SAW devices were prepared in the same manner on polished ST-cut quartz.[3] Before each experiment all wafers and devices were cleaned in a low-energy Ar plasma cleaner at medium power for 1 min (Harrick Scientific Corporation, NY, model PDC-32G).

Chemicals. Chemicals were generally of reagent-grade quality or better and used as received. However, most of the mercaptans were purified prior to use by sublimation or distillation. Poly(amidoamine) Starburst (PAMAM) dendrimers were used as received from Dendritech, Inc. (Midland, MI).

Characterization. FTIR-external reflection spectroscopy (FTIR-ERS) measurements were made using a Digilab FTS-40 spectrometer equipped with a Harrick Scientific Seagull reflection accessory and a liquid-N_2-cooled MCT detector. All spectra were the sum of 256 individual scans using *p*-polarized light at an 84° angle of incidence with respect to the substrate normal.[3]

In-situ polarization modulation FTIR (PM-FTIR) spectroscopic measurements were made using a modified Mattson Research Series 1 infrared spectrometer (ATI Inc., Madison, WI).[4,5] The infrared beam is passed through a ZnSe polarizer and a ZnSe photoelastic modulator (Hinds, model PEM90II/ZS37), reflected off the sample surface at an incident angle of 80°, passed through a focusing lens, and finally directed into a liquid N_2-cooled MCT detector. The photoelastic modulator is used to modulate the incident beam between *s*- (perpendicular) and *p*- (parallel) polarization with respect to surface normal. The real-time sampling electronics

(Mattson) ratio the surface-insensitive *s*-polarized signal to the surface-sensitive *p*-polarized signal. This method eliminates the need for a background spectrum.[6] A custom-built vapor-phase flow cell was employed for all PM-FTIR measurements; it has been described in detail previously.[7] The partial pressure of the analyte and the flow rate of the gas stream were determined by two mass-flow controllers: one controls an analyte-saturated N_2 vapor stream and the other a pure N_2 gas stream, which is used to reduce the concentration of the saturated analyte vapor. The total flow rate was set at 0.5 l/min for all experiments and the temperature was 23.5 ± 1 °C. PM-FTIR spectra of SAMs were obtained prior to dosing and subtracted from spectra obtained during dosing. Displayed spectra consist of 20 co-added cycles and each cycle consists of 100 sum and 200 difference scans; total acquisition time was about 47 min per spectrum. The resolution of all PM-FTIR spectra is 2 cm^{-1}.

SAW device measurements were made at 25 ± 0.5 °C using 2 (98-MHz) ST-cut quartz oscillators housed in a custom-built flow system.[8-10] Modified SAW devices were dosed with VOCs mixed down in N_2 as described for the PM-FTIR experiments. The change in SAW-device frequency (Δf), due to the adsorption of vapor-phase molecules, is related to the mass loading per unit area (m_a) through the equation $\Delta f/f_o = -\kappa c_m f_o m_a$. Here, f_o is the SAW oscillation frequency (98 MHz), κ is the fraction of the distance between the centers of the transducers covered by the Au film

(0.7) and c_m is the mass sensitivity coefficient of the device (1.33 $cm^2/(g \cdot MHz)$ for ST-cut quartz).

Results and Discussion

Monolayers. Monolayer self-assembly chemistry is useful for constructing functional organic surfaces.[11-13] For example, monolayers of *n*-alkanethiols spontaneously adsorb to Au from liquid and vapor phases.[12-16] The resulting monolayer assumes a $(\sqrt{3}x\sqrt{3})R30°$ overlayer structure on Au(111) (Scheme 1). Analyses indicate that this class of self-assembled monolayer (SAM) is composed of hydrocarbon chains tilted about 30-40° from the surface normal; SAMs prepared from shorter chains are more disordered than those formed from longer-chain molecules, and defects are thought to result primarily from gauche conformations within the energetically more favorable all-trans, extended SAM structure. SAMs are robust under normal laboratory conditions. [12-16]

Scheme 1

SAMs typically, but not always, derive their chemical selectivity from the outermost few angstroms of the film, which generally corresponds to the terminal functional groups.[16-18] Terminal groups, and thus chemical sensitivity, can be manipulated either prior to surface immobilization [16-18] or by chemical reaction following self assembly of a suitable adhesion layer.[3,19-21] SAM interfaces have the advantage of being easily and reproducibly

synthesized, and since analytes do not have to transfer through a diffusion barrier such as would be the case for a thicker polymer film, the sorption rate is typically rather fast. There are two principal disadvantages to the use of monolayer films, however. First, the level of synthetic flexibility is rather low, and therefore the degree of chemical independence that can be engineered into a simple SAM may not be as great as in thicker or more complex materials. Second, the total number of receptors incorporated into the film, and thus the dynamic range and sensitivity of the sensor, is limited by the surface area of the substrate.

SAMs prepared from carboxylic acid-functionalized organomercaptans provide a very simple illustration of how monolayers can be tailored to achieve chemical selectivity. The terminal acid groups interact with acidic or basic vapor-phase molecules by hydrogen bonding interactions or by proton-transfer reactions, respectively.[22,23] Hydrogen-bonding systems are typified by the interactions of *n*-alkanoic acids ($CH_3(CH_2)_nCOOH$, n=0-14) with Au surfaces modified with 3-mercaptopropionic acid ($Au/HS(CH_2)_2COOH$) (Scheme 2).

Scheme 2

Figure 1 shows FTIR-ERS data for $Au/HS(CH_2)_2COOH$ and $Au/HS(CH_2)_2CH_3$ surfaces after and before exposure to a saturated vapor of myristic acid, $CH_3(CH_2)_{12}COOH$. Prior to $CH_3(CH_2)_{12}COOH$

dosing, the Au/$HS(CH_2)_2COOH$ spectrum, Figure 1b, reveals bands due to the acid C=O stretch and the enhanced α-CH_2 scissors mode at 1722 and 1410 cm^{-1}, respectively. After dosing, the presence of a second surface-confined $CH_3(CH_2)_{12}COOH$ layer (Scheme 2) is confirmed by the appearance of the methyl C-H stretching vibration at 2964 cm^{-1}, the increased intensity of the methylene C-H stretching vibrations at 2929 and 2858 cm^{-1}, and the doubling of the intensity of the C=O stretching vibration at 1717 cm^{-1} (Figure 1a). The positions of the carbonyl bands in these two spectra indicate that the myristic acid is bound to the SAM by strong hydrogen bonds as indicated in Scheme 2.

Figure 1

To demonstrate that the acid-terminated SAM specifically selects for other acids, we also exposed a methylated surface to vapor-phase *n*-alkanoic acids as shown on the right side of Scheme 2. The FTIR-ERS spectrum of a surface-confined monolayer of $HS(CH_2)_2CH_3$ is shown in Figure 1d. The bands at high energy result from hydrocarbon stretching modes. Other peaks attributable to hydrocarbon backbone modes are also present at lower frequencies. The FTIR-ERS spectrum of the methyl surface after exposure to $CH_3(CH_2)_{12}COOH$, Figure 1c, is identical to the surface before acid dosing. This result clearly shows that only the acid surface is selective for acid-functionalized analytes and thus that these two

sensor surfaces respond very differently to the chemical class of acidic materials.

Simple Bilayers. Self-assembled films of complex molecules and molecular assemblies are generally more difficult to prepare than simple alkyl-based materials. However, step-wise self assembly of simple materials can lead to more complex systems. For example, it is possible to use a simple organomercaptan SAM as an adhesion layer to introduce additional complexity into an interfacial material. A very simple chemical trick can greatly expand the scope and versatility of the just-described acid-terminated SAM. The coating design discussed in this section takes advantage of the affinity of the deprotonated form of the acid-terminal groups of mercaptoundecanoic acid (MUA) for many different metal ions, including Ag^{+}, Cu^{2+}, Ni^{2+}, and Zn^{2+}, to yield a host of different chemically selective metal-carboxylate interfaces. Some of these interact strongly with organophosphonates such as the nerve-agent simulant diisopropylmethylphosphonate (DIMP) and presumably the Type G nerve agents it mimics. We chose to examine the Au/MUA-Cu^{2+} interface in detail because Cu^{2+} is a hydrolysis catalyst for certain nerve agents,[24] and we reasoned that materials that are good catalysts would also perform well as sensor materials for two reasons: catalyst/substrate interactions are typically selective and necessarily reversible.

The metal-ion/acid bilayers are very easy to prepare. The MUA monolayer is assembled by soaking a Au substrate in a dilute ethanolic solution of MUA for a few hours (or longer), then dipping it into a dilute ethanolic solution of the metal ion for a few

minutes, rinsing with ethanol, and drying. We have examined seven different metal-ion-capped SAM surfaces (Au/MUA-M^{n+}), but the discussion here is limited to Cu^{2+}. The formation of a MUA-Cu^{2+}-terminated monolayer, such as that illustrated at the top of Scheme 3, is easily confirmed by X-ray photoelectron spectroscopy (XPS) surface analysis and the replacement of the carbonyl band in the FTIR-ERS spectrum by carboxylate bands present at substantially lower energy.

Figure 2a presents nanogravimetric SAW data (frequency shift as a function of vapor-phase concentration) for six different organic analytes, as well as water, interacting with a MUA-Cu^{2+} SAM.[25] The adsorption isotherms in Figure 2a indicate that multilayers form (based on molar volumes of the bulk liquids) on the surface at 50%-of-saturation vapor pressure (p/p_{sat} = 0.5) for all the analytes examined except *i*-octane. The number of multilayers that adsorb gives a qualitative indication of the "range" of the monolayer/analyte interaction. It is thus interesting to note that the frequency shift for DIMP at 50% of saturation is consistent with the adsorption of approximately 17 layers of DIMP. This value is significantly larger than acetone, which has the next-highest equivalent molecular coverage (about 9 monolayers). DIMP forms multilayers at the lowest analyte partial pressure.

Figure 2

In contrast to the results for the MUA-Cu^{2+} surface, the same group of analytes interacting with a methyl-terminated SAM yield much lower adsorbed masses. As illustrated in Figure 2b, for example, there is no clear preference for the methyl-terminated surface by the organophosphonate. The same scales are used in both parts of Figure 2 to facilitate direct comparison of the two monolayer films. Non-specific interactions between the analyte and the monolayer film (i.e., van der Waals forces) as well as specific interactions between adsorbing analyte molecules account for the relative differences in adsorbed mass. The point is that simple surface engineering gives rise to a distinct difference in chemical selectivity. Moreover, there is the unanticipated result that many monolayers of DIMP adsorb to the MUA-Cu^{2+} surface, which enhances both the dynamic range of the sensor and its sensitivity. We thought it would be useful to better understand these intriguing results.

Figure 3 shows PM-FTIR difference spectra of a MUA-Cu^{2+} SAM during dosing with 10%- and 50%-of-saturation DIMP (parts a and c, respectively) and after purging with N_2 for 30 min (parts b and d). During dosing with 10%-of-saturation DIMP, several spectral features indicate strong interactions between vapor-phase DIMP and the composite film. First, the intense band present at 1079 cm^{-1} corresponds to the P=O stretching mode of metal-ion-complexed DIMP. It is known that the phosphoryl oxygen of many phosphorus-containing compounds coordinate with metal ions to yield adducts characterized by a dramatic shift to lower energy of this

band.[26-29] Typically, the metal-ion-complexed P=O band lies between 1100 and 1215 cm^{-1} depending upon the phosphorus compound, metal ion, and counter ion.[26-28] Our data for many MUA-M^{n+} surfaces indicate a shift to between 1060-1090 cm^{-1} for the P=O band. We attribute this larger shift to the substantial differences between the SAM surfaces discussed in this work and the ionic solids described earlier. [26-29]

Figure 3

Bands corresponding to the conversion of the carboxylate salt (negative bands at 1592 and 1437 cm^{-1}), arising from the strong Cu^{2+}-$(COO^{-})_2$ interaction, to the acid form of MUA (positive acid-carbonyl band at 1737 cm^{-1}) are also observed upon dosing with DIMP. Although the negative carboxylate bands are broad and somewhat indistinct in Figure 3, they are much sharper and intense for some of the other metal-ion-terminated SAMs we have examined.[5] Finally, a variety of other bands directly attributable to the C-H and O-C modes of DIMP are present in the spectrum of the MUA-Cu^{2+} surface.

We interpret the four spectra shown in Figure 3 in terms of the model illustrated in Scheme 3. Prior to DIMP exposure (top frame of Scheme 3) MUA is complexed to Cu^{2+}, which bears coordinating water ligands. Upon exposure to DIMP (middle frame), we propose that the carboxylate surface becomes protonated, accounting for the observed spectral changes in the MUA acid-group

bands discussed earlier, as a consequence of the very strong interaction between DIMP and Cu^{2+}. That is, Cu^{2+} complexed to the carboxylate groups prior to dosing binds to DIMP during dosing, and the resulting $-COO^-$ groups are protonated by water originally ligated to Cu^{2+} or otherwise introduced onto the high-energy MUA-Cu^{2+} surface (e.g., as an impurity in the (undistilled) DIMP). The result of this reaction gives rise to a Cu^{2+}/DIMP complex on the MUA surface, which is presumably charge compensated by nearby hydroxyl ions formed by the same reaction that leads to MUA protonation. DIMP now interacts both through hydrogen bonding with the MUA surface, as we have observed on MUA-only (no Cu^{2+}) SAMs,[5] and by coordinative interactions with Cu^{2+}. These aspects of the model are supported, respectively, by the presence of the hydrogen-bonded P=O band centered at 1214 cm^{-1} (parts a and c of Figure 3, dashed line), and the greatly shifted P=O band at 1079 cm^{-1} arising from Cu^{2+}-complexed DIMP.

Scheme 3

The reaction between DIMP and the MUA-Cu^{2+} surface is partially irreversible. This is apparent because most of the key bands shown in part a of Figure 3 are still present after purging with N_2 (part b). Indeed, some of these bands actually increase after purging with N_2 for 30 min. The origin of this enhancement is not clear, but it is fully reproducible after the first DIMP exposure, suggesting that it might arise from a reversible

orientational change of the P=O dipole or a change in the absorption coefficient of this band.[6]

An additional important spectral change occurs in the after-N_2-purging spectrum that supports the model shown in Scheme 3. Upon exposure to N_2, the carbonyl band, present after dosing with 10%-of-saturation DIMP at 1737 cm^{-1}, splits into a doublet having peaks centered at 1737 and 1710 cm^{-1}. We attribute the doublet to the removal of DIMP bound to the MUA surface through the relatively weak hydrogen-bonding interaction. Accordingly, as shown in the bottom frame of Scheme 3 and signaled by the new 1710 cm^{-1} band, the MUA SAM regains its intramonolayer lateral hydrogen bonds.[22]

When the surface is dosed with a higher concentration of DIMP after N_2 purging (part c of Figure 3) several spectral changes consistent with Scheme 3 are observed. First, all of the peak intensities arising from DIMP increase substantially (note the change of scale) except the Cu^{2+}-associated P=O band (1079 cm^{-1}), which remains constant. This indicates that whatever concentration of Cu^{2+}-complexed DIMP is present on the surface after initial 10%-of-saturation exposure survives N_2 purging and cannot be increased by increasing the vapor-phase concentration of DIMP. In other words, after the initial dosing, all Cu^{2+} sites remain coordinated to DIMP for the duration of the experiment. Second, note that the carbonyl band arising from laterally hydrogen bonded MUA acid groups is diminished upon dosing with 50%-of-saturation DIMP. This is a consequence of the lateral MUA

hydrogen bonds being replaced with DIMP/MUA hydrogen bonds as indicated by the return of the corresponding peak at 1214 cm^{-1} in part c of Figure 3. Third, a new peak, not originally present at low dosing concentration, appears at 1246 cm^{-1}. This band arises from the P=O stretching mode of uncomplexed DIMP, and its position is consistent with that found for the bulk liquid phase (1245 cm^{-1}).

There are three important conclusions that arise from these DIMP dosing experiments. First, a synthetic step as simple as dipping a SAM into a metal-ion-containing solution yields a composite interface with significantly different selectivity and sensitivity. We have shown previously that the DIMP response is a strong function of the type of metal ion.[5] Second, the proper analytical tools, SAW devices and PM-FTIR spectroscopy in this case, yield real-time information that can be used to fully define the analyte/monolayer interaction chemistry. This is essential for optimizing and discovering new interfacial materials. Third, even though it is reasonable to assume that the surface receptors would saturate after adsorption of one or two monolayers of analyte, at least in this case saturation does not occur even after more than 17 monolayer-equivalents of DIMP adsorb to the surface. As discussed in the next section, the latter important result appears to be somewhat general.

Complex Bilayers. The metal-ion-terminated SAMs discussed in the previous section provide good selectivity and sensitivity; however, we thought it would be possible to gain additional control over selectivity by developing more complex bilayer

structures. The prototype for this approach is calixarene (CA[n])-functionalized SAMs (Scheme 4). CA[n] belong to a class of bucket-shaped molecules consisting of n (= 4-11) phenyl subunits.[30] In the cone conformation,[30] CA[4] and CA[6] have inner cavity diameters of 6.3 Å and 7.9 Å, and outer upper-rim diameters of 13.6 Å and 18.0 Å, respectively.[31] The host-guest interactions associated with the hydrophobic CA[4] and CA[6] cavities are usually weak, since they involve principally van der Waals, induced-dipole, and π-stacking interactions. A resilient intermediate adhesion layer based on photopolymerized diacetylenic SAMs, rather than the simple *n*-alkylthiols described in the previous sections, was used for this study to enhance bilayer stability (Scheme 4).[32] In this section, we discuss the linking chemistry that leads to calixarene immobilization and examine the role the calixarene cavities play in recognizing six volatile organic compounds (VOCs) using SAW device-based gravimetry.

Scheme 4

Part I of Scheme 4 illustrates the synthesis of the polydiactylene/calixarene (PDA/CA[n]) bilayers.[3] Monolayers were prepared by soaking a Au substrate in a solution of the acid-terminated diacetylene, and then polymerizing with UV light. [33] Following polymerization, the substrates were exposed to $SOCl_2$ vapor to convert the carboxylic acid functional groups to the more reactive acid chloride (PDA-COCl). CA[4] and CA[6] are bound to

PDA-COCl through a covalent ester linkage via the hydroxyl groups on their lower rim.

Part II of Scheme 4 illustrates the irreversible adsorption of vapor-phase *n*-butylamine onto the CA[n] bilayer-coated SAW devices. We use this as an indirect nanogravimetric method to approximate the fractional surface coverage of CA[n] on the PDA surface. By measuring the difference in *n*-butylamine mass loading on the PDA-COOH and PDA/CA[n] surfaces we calculate that CA[4] and CA[6] cover 58% and 61%, respectively, of the PDA-COOH surface.[3] The irreversibly bound *n*-butylamine serves a secondary purpose by effectively filling voids between calixarenes, thereby hindering VOC access to these domains.

Figure 4 shows a summary of the average mass-loading data obtained from dosing the PDA-COOH and PDA-CH_3 monolayer- and PDA/CA[4] and PDA/CA[6] bilayer-coated SAW devices with six VOCs. The bilayer-coated devices generally yield higher mass-loading responses relative to the PDA-only-coated devices. We anticipated this result because of the enhanced binding between the calixarene cavities and VOCs compared to their nonspecific interactions with the PDA-CH_3 and PDA-COOH surfaces.

Figure 4

Dosing the bilayer-coated SAW devices with VOCs before and after exposure to *n*-butylamine allows us to better understand the role of the calixarene cavities, relative to non-specific adsorption at, for example, defect sites between CA[n] molecules.

Frequency shifts associated with analyte dosing of the CA[4]- and CA[6]-coated devices before and after irreversible adsorption of *n*-butylamine are within 5% of a monolayer for all six VOCs. This strongly suggests that enhanced VOC adsorption at the calixarene-modified surface results from the cavities rather than interstitial voids.

Figure 5 shows a summary of the average mass-loading data obtained from dosing thiophenol (TP)-, phenyl-terminated PDA (PDA/Ph)-, 4-*tert*-butylphenyl-terminated PDA (PDA/*t*-Ph)-, PDA/CA[4]-, and PDA/CA[6]-coated SAW devices with 25%-of-saturation benzene, toluene, and CCl_4. The TP, PDA/Ph, and PDA/*t*-Ph control surfaces were chosen because of their chemical similarity to the surfaces of the PDA/CA[n] bilayers, but note the absence of a structurally distinct cavity on the control surfaces. TP is bound to the Au substrate directly through a thiolate interaction while Ph and *t*-Ph are linked to the PDA layer through ester linkages in the same manner as CA[n].

Figure 5

We dosed the TP, PDA/Ph, and PDA/*t*-Ph surfaces to determine whether VOC adsorption is enhanced at the CA[n] surfaces on the basis of specific interactions with discrete CA[n] macrocycles or whether non-specific interactions, promoted by the calixarene *t*-butylphenyl groups, dominate adsorption. Referring to Figure 5, the magnitude of VOC adsorption is much smaller, typically less than 50%, for the TP, PDA/Ph, and PDA/*t*-Ph surfaces compared to

the PDA/CA[n] bilayers. We would expect that if the adsorption enhancement observed for the CA[n] surfaces results primarily from nonspecific interactions between the VOCs and the functional groups on the CA[n] upper rim, then a similar extent of VOC adsorption would occur at these control surfaces.

On the basis of the data in Figure 5, we conclude that the calixarene cavities figure prominently in the chemical selectivity of these interfaces. Evidence for this comes from the enhanced adsorption noted for benzene and toluene on the CA[n] surfaces compared to TP, PDA/Ph, and PDA/*t*-Ph surfaces. The CA[4] and CA[6] cavities have interior diameters of 6.3 Å and 7.9 Å, respectively. The benzene and toluene molecules have estimated molecular diameters, across the 2,6 hydrogens, of 6.3 Å (CPK models) and their flat, discus-like shapes are conducive to inclusion within the CA[n] cavities. Thus, we conclude that enhanced selectivity for benzene and toluene results from a favorable specific interaction between the hydrophobic cavities of the two calixarenes and the two aromatic compounds. Additional evidence for analyte inclusion into the calixarenes comes from a comparison of the CCl_4 data (Figure 5). The PDA/CA[6] bilayer is significantly more receptive to the CCl_4 probe than the PDA/CA[4], PDA/*t*-Ph, PDA/Ph, or TP surfaces. We interpret this result in terms of size and shape selectivity. Unlike benzene or toluene, CCl_4 has spherical symmetry and is too large, (approximately 6.4 Å in diameter based on CPK models), to fit entirely within the CA[4] cavity, but it is sufficiently small to be accommodated by CA[6].

There is one final very interesting issue raised by the data in Figure 5. As discussed earlier, CA[4] and CA[6] have estimated surface coverages of 58% and 61%, respectively, which corresponds to 0.06 nmol/cm^2 and 0.04 nmol/cm^2, respectively. Dosing the CA[4] and CA[6] surfaces with 25%-of-saturation benzene yields mass loadings of 0.70 and 0.97 nmol/cm^2, respectively. Since a 1:1 host:guest stoichiometry would yield maximum benzene coverages equal to the CA[4] and CA[6] surface concentrations, we conclude that the calixarenes act as templates that nucleate benzene into clusters that average 10-20 molecules each and permit it (as well as some of the other probe molecules) to adopt surface conformations that are to some degree solid-like. That is, the phase of the surface-confined benzene must have a lower vapor pressure than liquid benzene, otherwise it would immediately desorb at the partial benzene pressure used for these experiments. Importantly, on the three non-calixarene surfaces shown in Figure 5, the surface concentration of benzene does not exceed half of the maximum single-monolayer coverage (roughly the same as the PDA monolayer: 0.94 nmol/cm^2), which provides an important control that strongly suggests the fully reproducible data for CA[4] and CA[6] surfaces is correct. Note that this is precisely the same type of nucleation effect observed for the MUA-Cu^{2+} bilayers described in the previous section, which gives us confidence that this phenomenon might be quite general and useful for sensor applications.

Dendrimers. Dendrimers are polymers prepared by repetitive branching from a central core (left side of Scheme 5).[34] They have

three distinct structural features: a core, repetitive branch units (dendrons) and terminal functional groups. Dendrimer size increases with generation number and its molecular conformation evolves. At generation 0 or 1 (G0 or G1), most dendrimers have an expanded or 'open' configuration, but as they grow in size, crowding of the surface functional groups cause the dendrimer to adopt a spherical or globular structure. As illustrated by the dendrimer branch shown in Scheme 6, surface-confined dendrimers have several attractive attributes for sensing applications. First, they are dense on the outside but somewhat hollow on the inside. This means that VOCs can sorb into the interior of the dendrimer and be size selected by synthetically controlling the dimensions of the pores that result from packing of the outermost branches. Second, the chemical identity of both the exterior and interior of the dendrimer can be tailored for specific applications, which greatly enhances molecular specificity. Finally, dendrimers are three-dimensional objects, so they are inherently more highly functionalized than the *n*-alkylthiol SAMs and SAM-based bilayers described previously. This leads to increased sensitivity and synthetic flexibility.

Scheme 5

Scheme 6

There are several methods appropriate for attaching dendrimers to surfaces for chemical sensing applications. For example, we recently discovered that amine-terminated

poly(amidoamine) (PAMAM) dendrimers strongly adsorb directly to Au in near-monolayer coverages.[35] Alternatively, dendrimers can be anchored to surfaces via SAM adhesion layers.[19,36] For example, activation of the terminal groups of a MUA SAM followed by exposure to a PAMAM dendrimer leads to covalent attachment via amide linkages (Scheme 5). Spectroscopic analysis indicates that a severe distortion of the dendrimer, in the form of flattening, occurs upon immobilization either directly on Au or via the intermediate MUA adhesion layer. For example, immobilization of a G4 PAMAM dendrimer, which has a bulk-phase diameter of 4.5 nm, directly onto Au results in a decrease in the maximum per-dendrimer height to about 2.8 nm.[35] Obviously, this has a significant effect on the pore size and endoreceptivity of these materials (Scheme 6).

It is possible to reduce the magnitude of these morphological changes by using a mixed-SAM adhesion layer consisting of a small surface concentration of an *n*-alkylthiol terminated in a reactive group, such as a carboxylic acid, diluted by a much shorter, unreactive methyl-terminated *n*-alkylthiol.[36] Activation of the small percentage of acid groups using the chemistry illustrated in Scheme 5 results in linking of one or just a few terminal groups of each dendrimer to the surface. Distortion is avoided because the remaining terminal amine groups neither react with nor wet the dominant methyl-terminated component of the SAM. Regardless of the approach used, dendrimers have tremendous potential as interfacial materials for chemical sensing because of their shape and the high degree of synthetic flexibility inherent to their

many reactive sites.

To illustrate the suitability of dendrimer surfaces as chemically sensitive interfaces and demonstrate some of the principles that govern their performance, we sequentially dosed PAMAM dendrimer-modified SAW devices with VOCs having different functional groups (Figure 6).[19] These surfaces were prepared as illustrated in Scheme 5. Figure 6a is an example of unprocessed data from a typical SAW experiment. It illustrates how the dendrimer-modified device response possesses three of the essential attributes of an ideal chemical sensor: the response to dosants is very rapid with no detectable permeation transient, the signal-to-noise ratio is excellent, and the response is typically completely reversible.

Figure 6b summarizes the results of many dosing experiments like those just discussed. The response to VOCs decreases in the order acid > alcohols > hydrophobic dosants. This response order is more pronounced for the G4-G8 modified surfaces and is dictated by the PAMAM structure which possesses hydrogen-bonding exoreceptors and endoreceptors. The G4-modified surface is the most responsive material because, although it is the smallest of the spheroidal dendrimers (the G2 and G0 dendrimers are more-or-less flat), its interior endoreceptors are most accessible because of enhanced porosity compared to the more compact G6 and G8 dendrimer surfaces. G0 and G2 dendrimer films are not as effective at discriminating between the three different classes of analytes since these surfaces have few or no free amine terminal groups and no coherent endoreceptive ability. The important point

is that the chemical and structural characteristics of the dendrimers can be used to predict the classes of analytes they are likely to interact with.

Figure 6

Summary and Conclusions

Array-based chemical sensors are likely to play an increasing role in future analytical detection systems. The heart of these devices are the chemically sensitive materials affixed to the transducers, and chemists clearly have an expanding role to play in designing, characterizing, and testing these materials. Interfacial materials must be synthetically versatile so that classes of materials, like the SAMs and dendrimers described in this *Account*, can be easily and inexpensively manipulated synthetically to yield families of materials that provide chemically independent responses in the presence of target analytes. Additionally, attachment of the materials to suitable transducers must be straightforward. It is also advantageous to be able to predict the sensor response based on simple chemical principles and a knowledge of the structural and chemical properties of the interfacial material and analytes. For example, we predicted that the MUA-Cu^{2+} surface would preferentially bind DIMP because Cu^{2+} is a hydrolysis catalyst for Type G nerve agents. It also follows from chemical intuition that the responses of the PAMAM dendrimer interfaces to VOCs should follow the profile shown in Figure 6. Finally, the time response and sensitivity of the

interfacial materials must be considered. SAM monolayers generally provide very fast responses, but their sensitivity and dynamic range is restricted by the limited number of receptors inherent to a planar surface. Note, however, that our discovery that SAM receptors can bind analytes in a much-greater-than-1:1 stoichiometry provides some relief to this limitation.[3,25] Thicker materials such as polymers provide a much larger number of receptors, and thus enhance sensitivity compared to monolayers, but permeation transients may render them inappropriate for time-sensitive applications such as chemical weapons detection or high-throughput applications such as those associated with airport screening for illicit materials. Perhaps quasi-three-dimensional materials like the dendrimer monolayers or ultrathin layered materials will help to provide a compromise between time response and sensitivity in future-generation devices.

Acknowledgments

We acknowledge the hard work and intellectual contributions of our research group members past and present: Merlin L. Bruening, Daniel L. Dermody, Maurie E. Garcia, Larry J. Kepley, Taisun Kim, Laurel J. McEllistrem, Robert Peez, Li Sun, Mona Wells, Ross C. Thomas, Hideo Tokuhisa, Chuanjing Xu, and Huey Yang. The authors also gratefully acknowledge Mark Kaiser of Dendritech, Inc. (Midland, MI) for supplying samples of the Starburst PAMAM dendrimers. We also thank Professor Robert M. Corn for invaluable assistance in setting up the PM-FTIR experiment. Finally, the work at Texas A&M would not have been

possible without generous and sustained financial support from the National Science Foundation (CHE-9313441), the Office of Naval Research, the Robert A. Welch Foundation, and Sandia National Laboratories. Work at Sandia was supported by the United States Department of Energy under Contract DE-AC04-94AL85000. Sandia is a multiprogram laboratory operated by Sandia Corporation, a Lockheed-Martin Company, for the United States Department of Energy.

References and Notes

1. Ricco, A. J.; Crooks, R. M.; Osbourn, G. C., submitted for publication in *Acc. Chem. Res.*

2. Osbourn, G. C.; Bartholomew, J. W.; Ricco, A. J.; Frye, G. C., submitted for publication in *Acc. Chem. Res.*

3. Dermody, D. L.; Crooks, R. M.; Kim, T. *J. Am. Chem. Soc.* **1996**, *118*, 11912.

4. Barner, B. J.; Green, M. J.; Sáez, E. I.; Corn, R. M. *Anal. Chem.* **1991**,*63*, 55.

5. Crooks, R. M.; Yang, H. C.; McEllistrem, L. J.; Thomas, R. C.; Ricco, A. J., submitted for publication in *Faraday Disc.*

6. Porter, M. D., *Anal. Chem.* **1988**, *60*, 1143A.

7. Xu, C.; Sun, L.; Kepley, L. J.; Crooks, R. M.; Ricco, A. J. *Anal. Chem.* **1993**, *65*, 2102.

8. Ricco, A. J.; Frye, G. C.; Martin, S. J. *Langmuir* **1989**, *5*, 273.

9. Hughes, R. C.; Ricco, A. J.; Butler, M. A.; Martin, S. J. *Science* **1991**, *254*, 74.

10. Ricco, A. J. *The Electrochem. Soc. Interface* **1994**, *3*, 38.

11. Swalen, J. D.; Allara, D. L.; Andrage, J. D.; Chandross, E. A.; Garoff, S.; Israelachvili, J.; McCarthy, T. J.; Murray, R.; Pease, R. F.; Rabolt, J. F.; Wynne, K. J.; Yu, H. *Langmuir* **1987**, *3*, 932.

12. Ulman, A. *An Introduction to Ultrathin Organic Films From Langmuir-Blodgett to Self-Assembly*; Academic: San Diego, 1991.

13. Dubois, L. H.; Nuzzo, R. G. *Annu. Rev. Phys. Chem.* **1992**, *43*, 437.

14. Chailapakul, O.; Sun, L.; Xu, C.; Crooks, R. M. *J. Am. Chem. Soc.* **1993**, *115*, 12459.

15. Nuzzo, R.; Allara, D. L. *J. Am. Chem. Soc.* **1983**, *105*, 4481.

16. Bain, C. D.; Troughton, E. B.; Tao, Y.-T.; Evall, J.; Whitesides, G. M.; Nuzzo, R. G *J. Am. Chem. Soc.* **1989**, *111*, 321.

17. Chidsey, C. E. D.; Loiacono, D. N. *Langmuir* **1990**, *6*, 682.

18. Nuzzo, R.; Zegarski, B. R.; Dubois, L. H. *J. Am. Chem. Soc.* **1987**, *109*, 733.

19. Wells, M.; Crooks, R. M. *J. Am. Chem. Soc.* **1996**, *118*, 3988.

20. Zhou, Y.; Bruening, M. L.; Bergbreiter, D. E.; Crooks, R. M.; Wells, M. *J. Am. Chem. Soc.* **1996**, *118*, 3773.

21. Duevel, R. V.; Corn, R. M. *Anal. Chem.* **1992**, *64*, 337.

22. Sun, L.; Kepley, L. J.; Crooks, R. M. *Langmuir* **1992**, *8*, 2101.

23. Sun, L.; Crooks, R. M.; Ricco, A. J. *Langmuir* **1993**, *9*, 1775.

24. Wagner-Jauregg, T.; Hackley, B. E. Jr.; Lies, T. A.; Owens, O. O.; Proper, R. J. *Am. Chem. Soc.* **1955**, 77, 922.

25. Thomas, R. C.; Yang, H. C.; DiRubio, C. R.; Ricco, A. J.; Crooks, R. M. *Langmuir* **1996**, *12*, 2239.

26. Guilbault, G. G.; Scheide, E. P. *J. Inorg. Nucl. Chem.* **1970**, *32*, 2959.

27. Karayannis, N. M.; Pytlewski, L. L.; Owens, C. *J. Inorg. Nucl. Chem.* **1980**, *42*, 675.

28. Guilbault, G. G.; Das, J. *J. Phys. Chem.* **1969**, *73*, 2243.

29. Goodgame, D. M. L.; Cotton, F. A. *J. Chem. Soc.* **1961**, *3735* and references therein.

30. Gutsche, C. D. *Calixarenes*; The Royal Society of Chemistry: London, 1989.

31. The edge-to edge internal cavity diameters and the upper outer-rim diameters of CA[4] and CA[6], in the cone conformation, were estimated from CPK models.

32. Kim, T.; Chan, K. C.; Crooks, R. M. *J. Am. Chem. Soc.* **1997**, *119*, 189

33. Kim, T.; Chan, K. C.; Crooks, R. M.; Ye, Q.;Sun, L. *Langmuir* **1996**, *12*, 6065

34. Tomalia, D. A. *Sci. Am.* **1995**, *272*, 62.

35. Tokuhisa, H.; Zhao, M.; Baker, L. A.; Phan. V. T.; Dermody, D. L.; Garcia, M. E.; Peez, R.; Crooks, R. M. In preparation.

36. Tokuhisa, H.; Crooks, R. M. *Langmuir*, in press.

Figure Captions

Figure 1. FTIR-ERS spectra of a Au/$HS(CH_2)_2COOH$ surface before (b) and after (a) exposure to vapor-phase $CH_3(CH_2)_{12}COOH$. FTIR-ERS spectra of a Au/$HS(CH_2)_2CH_3$ surface before (d) and after (c) exposure to vapor-phase $CH_3(CH_2)_{12}COOH$. Only the acid-terminated SAM is receptive to binding of $CH_3(CH_2)_{12}COOH$, as indicated by the doubling of the carbonyl band at 1717 cm^{-1} and the increase of the methylene and methyl modes at high energy in part (a).

Figure 2. Adsorption isotherms for a SAW device coated with either a (a) MUA-Cu^{2+} or (b) CH_3-terminated SAM, exposed to six different organic analytes and water. Each isotherm was obtained over the course of 2 h. The same scales are used in both parts of the figure to directly compare the response of the two SAMs. In (a), the equivalent coverage for the DIMP analyte at 50%-of-saturation is about 17 layers. The MUA SAMs were allowed to form for 180 h.

Figure 3. PM-FTIR spectra of a MUA-Cu^{2+} SAM during dosing with (a) 10%- and (c) 50%-of-saturation DIMP, and then (b and d) purging with N_2 for 30 min. The dashed lines represent the hydrogen-bonded phosphoryl band at 1214 cm^{-1} and the non-hydrogen-bonded -COOH band at 1737 cm^{-1}. Note the change in scale for (c).

Figure 4. Comparison of the average mass loading per area for

PDA-CH_3-, PDA-COOH-, PDA/CA[4]-, and PDA/CA[6]-coated SAW devices exposed to six VOCs present at 25% of saturation in dry N_2.

Figure 5. Comparison of the average mass loading per area for TP-, PDA/Ph-, PDA/*t*-Ph-, PDA/CA[4]-, and PDA/CA[6]-coated SAW devices exposed to benzene, toluene, and CCl_4 present at 25% of saturation in dry N_2.

Figure 6. (a) Unprocessed response from a G8 PAMAM dendrimer-modified SAW device dosed with vapor-phase butanol. (b) Results from dosing dendrimer-modified SAW devices with six VOCs. Error bars represent the standard deviation of the average results from three devices, each cycled three times per dosant.

TOP VIEW

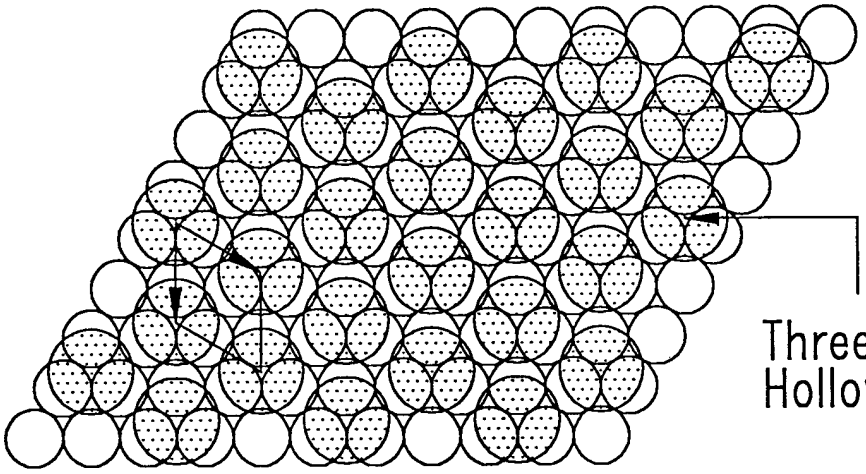

SIDE VIEW

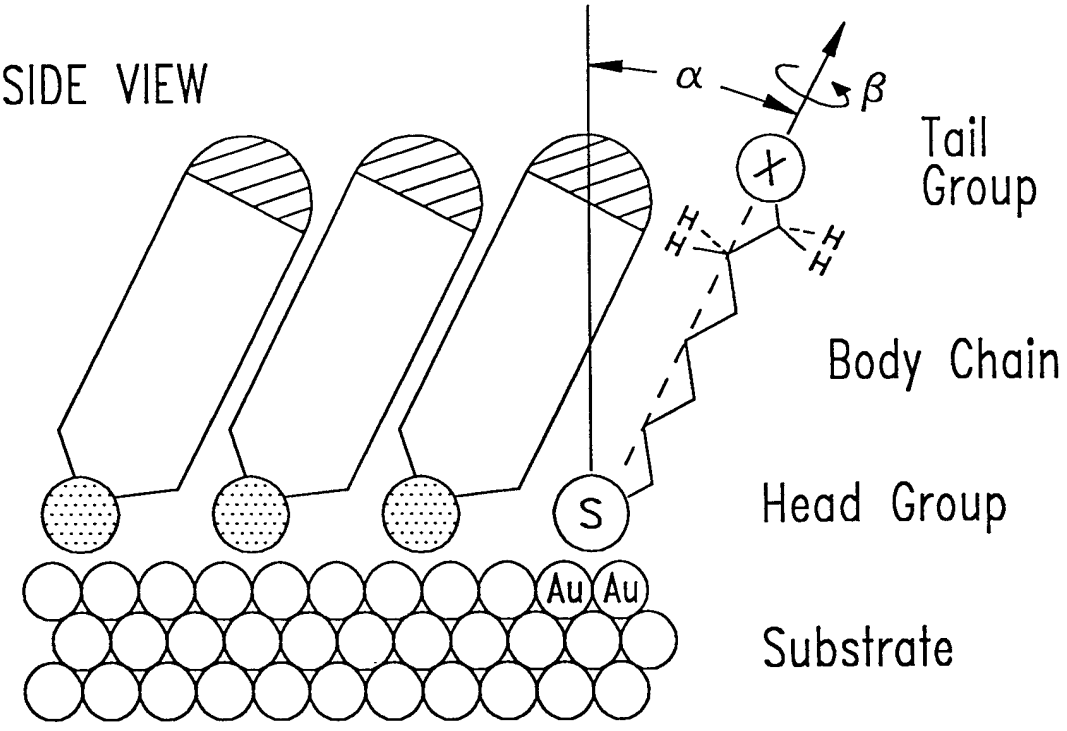

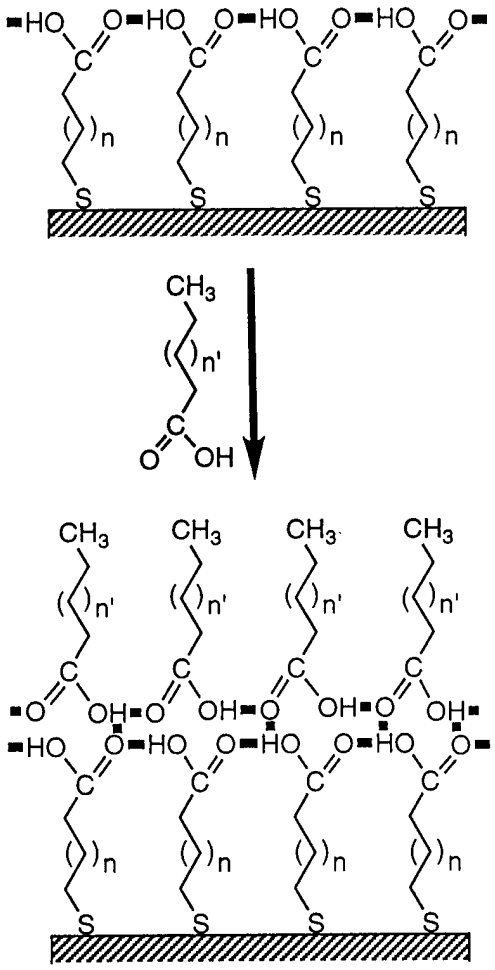

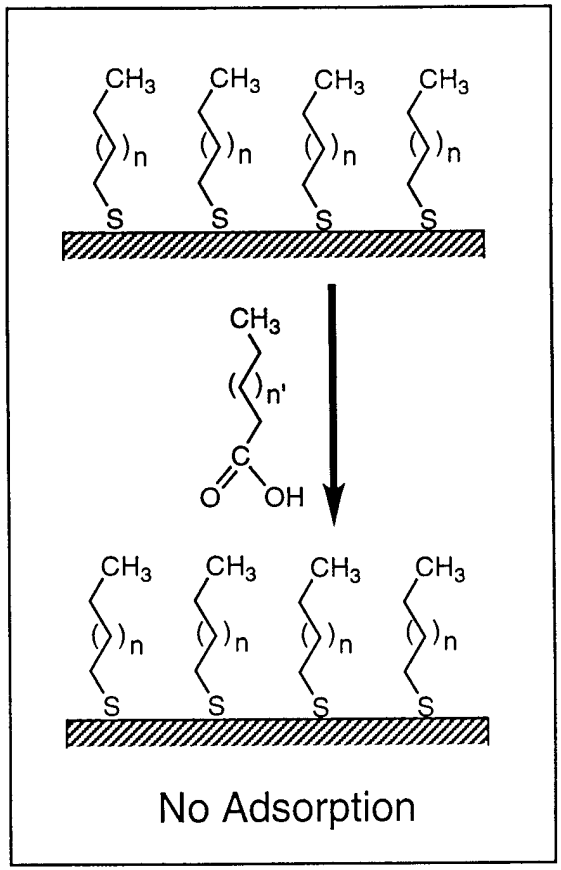

Scheme 2 / Crooks et al.

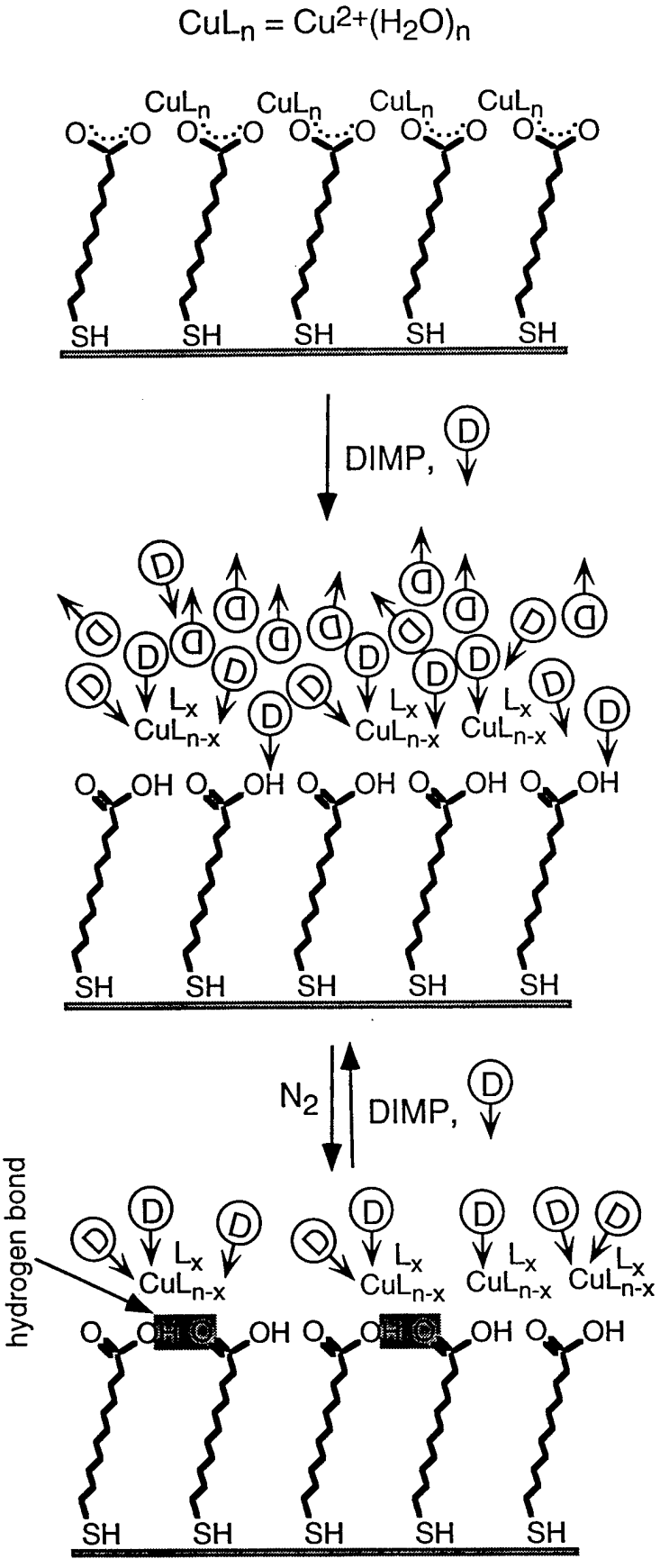

Scheme 3/Crooks et al.

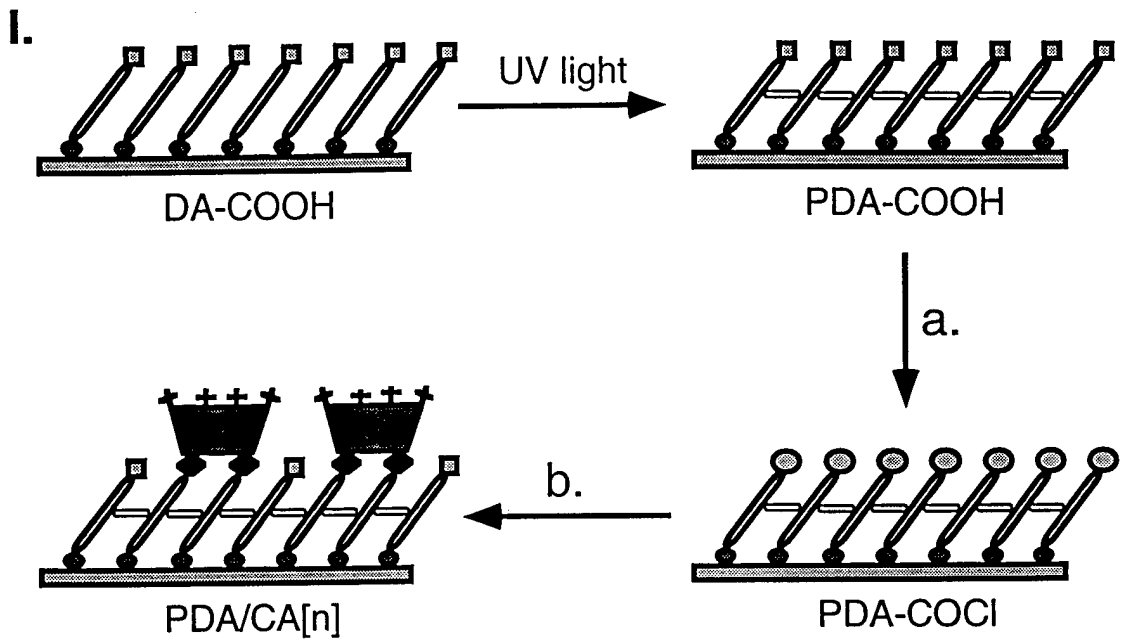

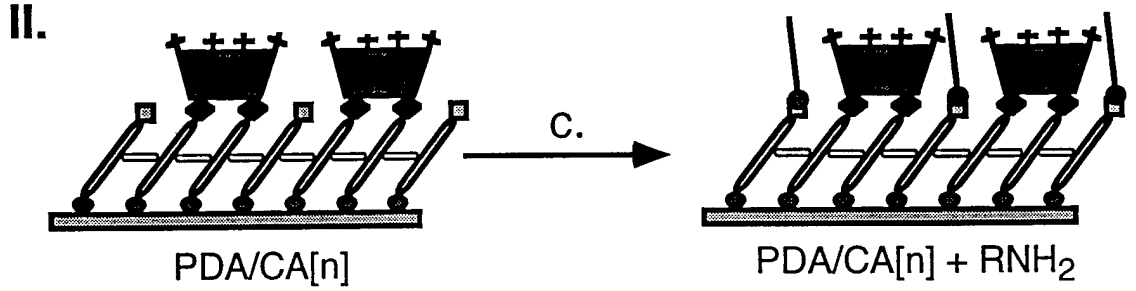

= $HS(CH_2)_{10}C{\equiv}CC{\equiv}(CH_2)_{10}COOH$; = $CH_3(CH_2)_3NH_2$

= $-\overset{O}{\overset{\|}{C}}OH$; = $-\overset{O}{\overset{\|}{C}}Cl$; = $-\overset{O}{\overset{\|}{C}}O$;

= *t*-butylcalix[4]arene (CA[4]) or *t*-butylcalix[6]arene (CA[6])

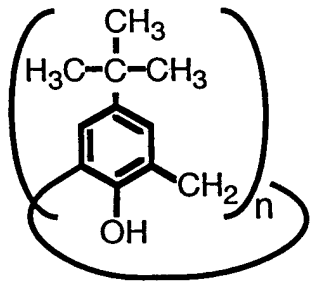

a. N_2, $SOCl_2$

b. CA[4] or CA[6], K_2CO_3, THF, T = 65-70 C

c. N_2, 25%-of-saturation *n*-butylamine, N_2

Scheme 4/Crooks et al.

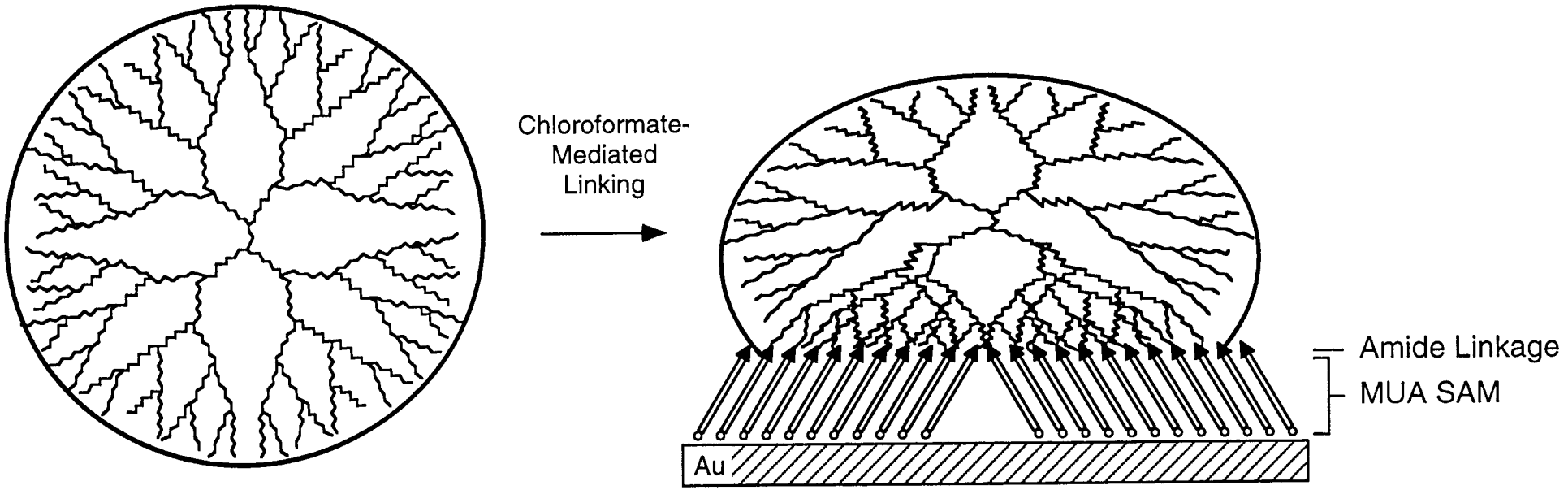

G4 PAMAM Dendrimer

Branches = $-N(CH_2CH_2CONHCH_2CH_2N-)_2$

Terminal End Groups = $-NH_2$

Scheme 5/Crooks et al.

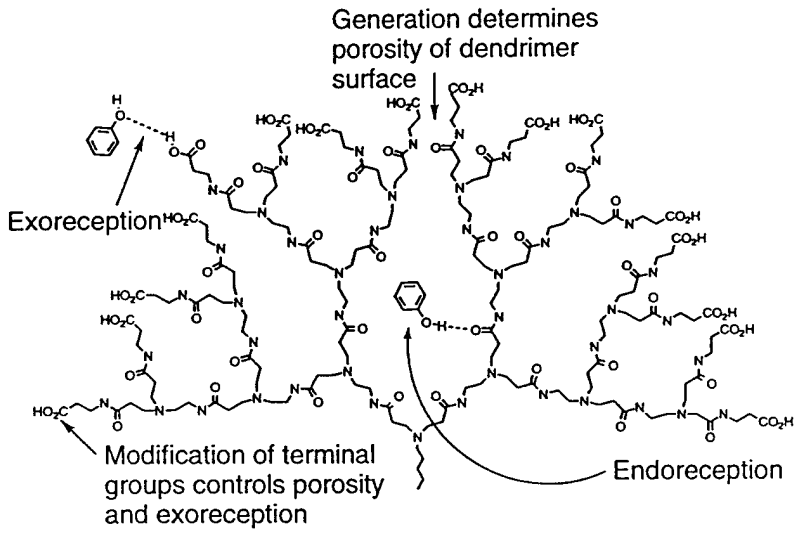

Scheme 6/Crooks et al.

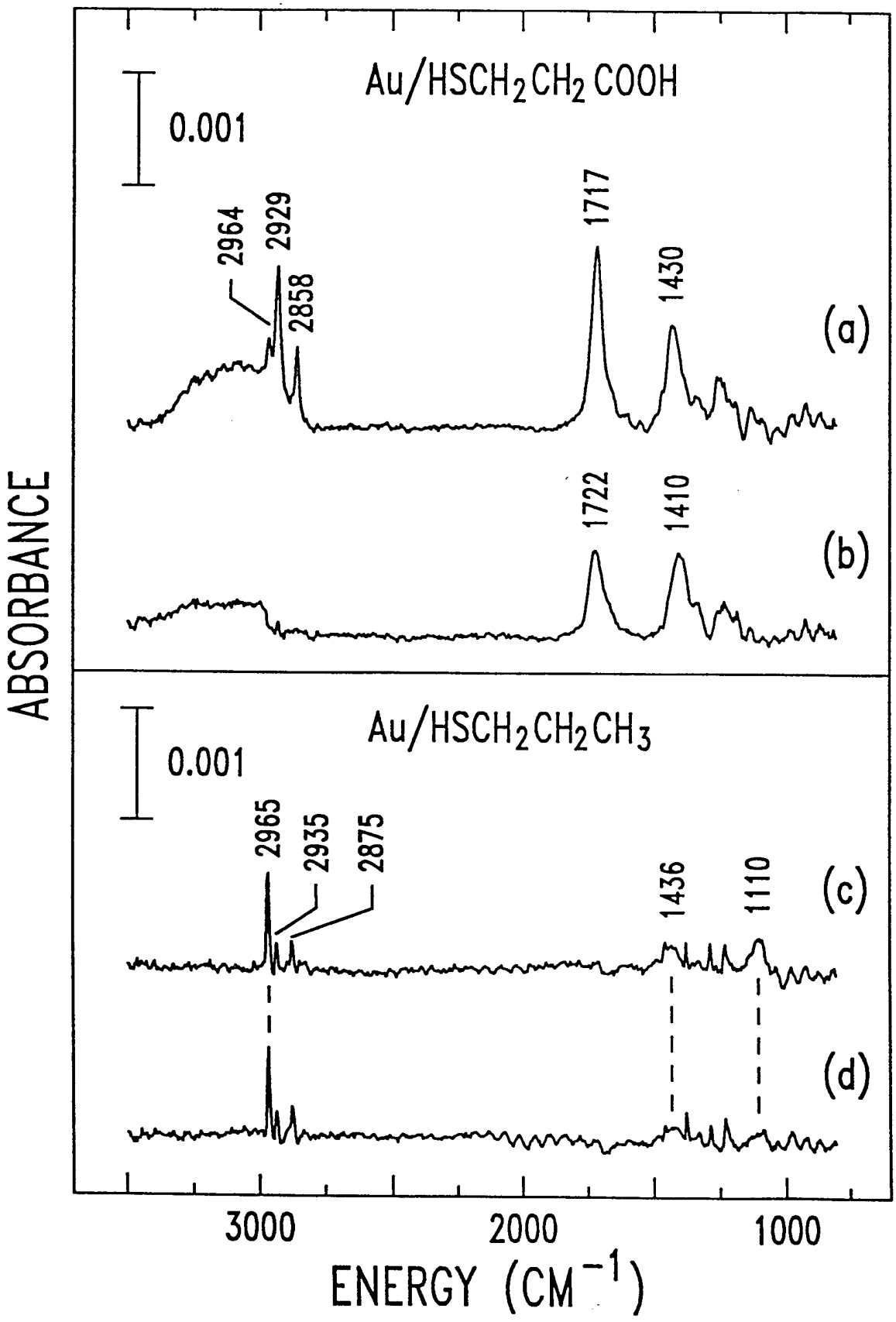
Au/HSCH2CH2COOH
0.001
2964
2929
2858
1717
1430
(a)
1722
1410
(b)
Au/HSCH2CH2CH3
0.001
2965
2935
2875
1436
1110
(c)
(d)
ABSORBANCE
3000
2000
1000
ENERGY (CM-1)

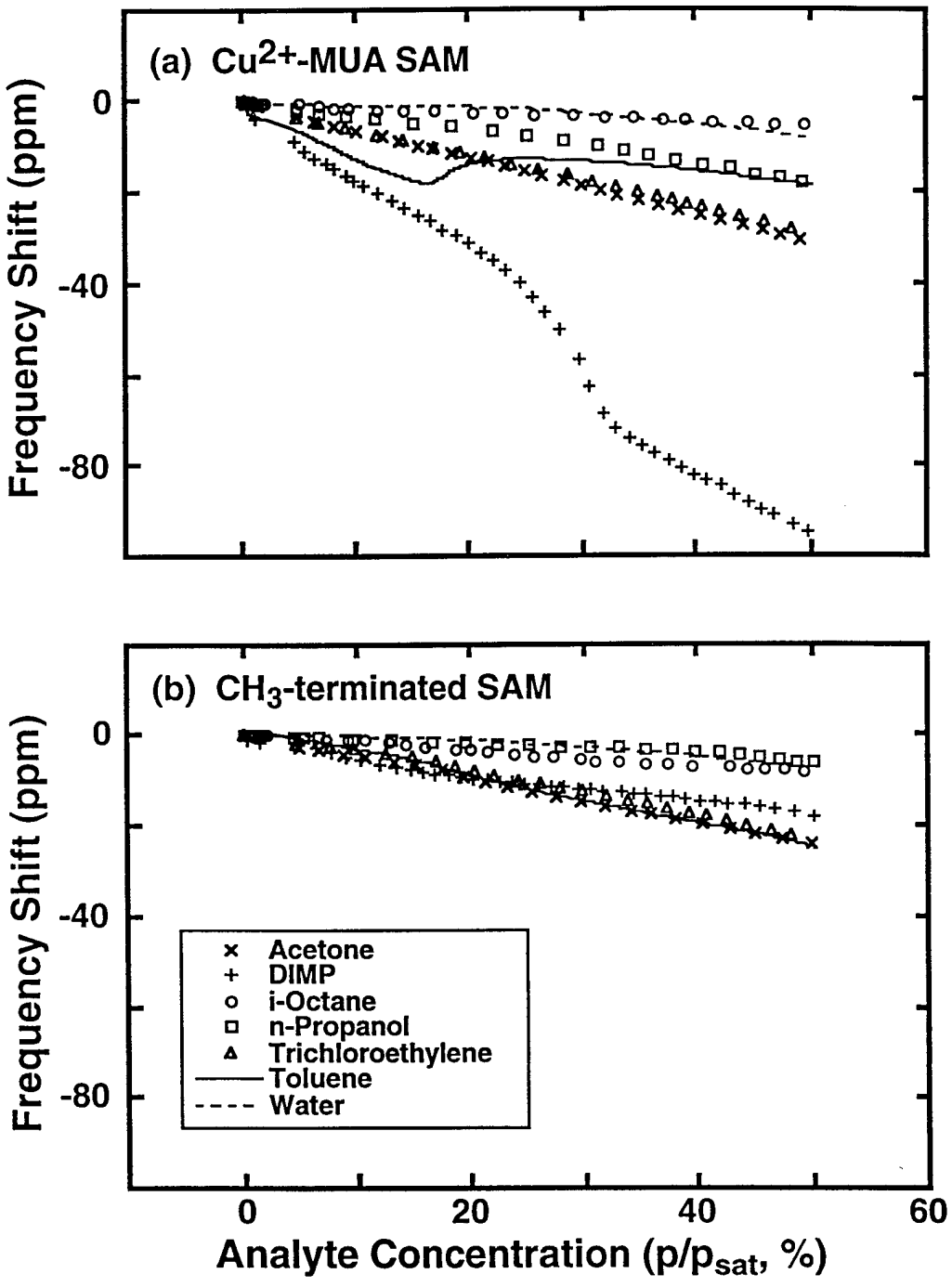

Figure 2/Crooks et al.

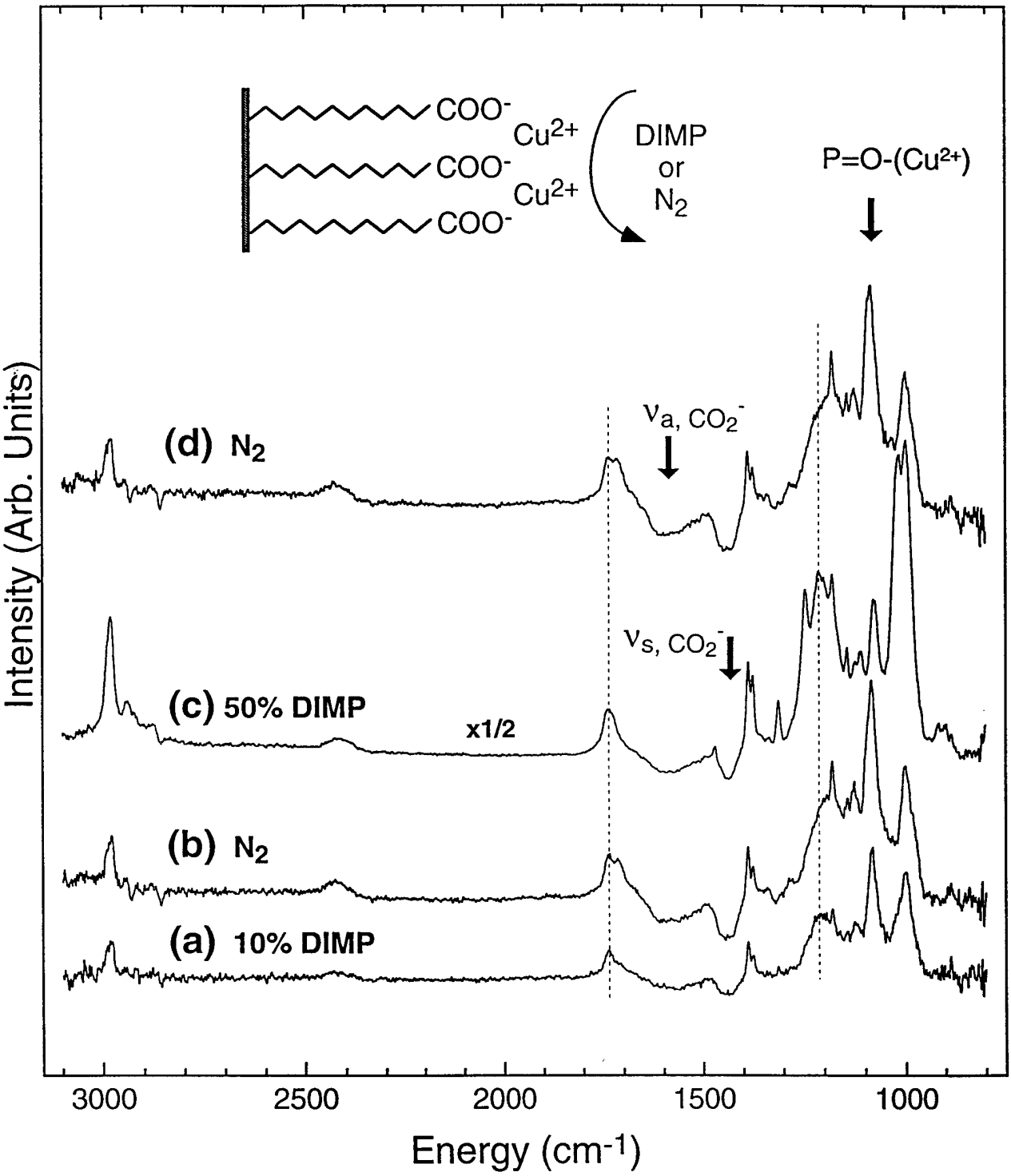

Figure 3 / Crooks et al.

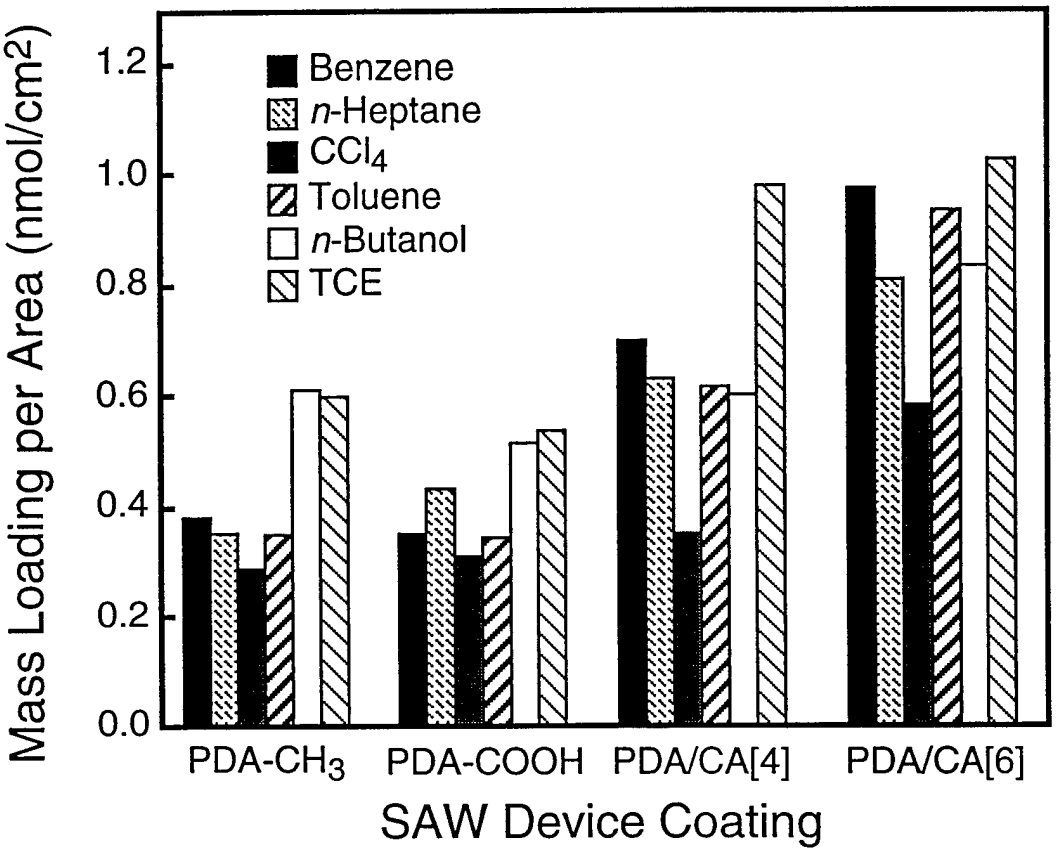

Figure 4/Crooks et al.

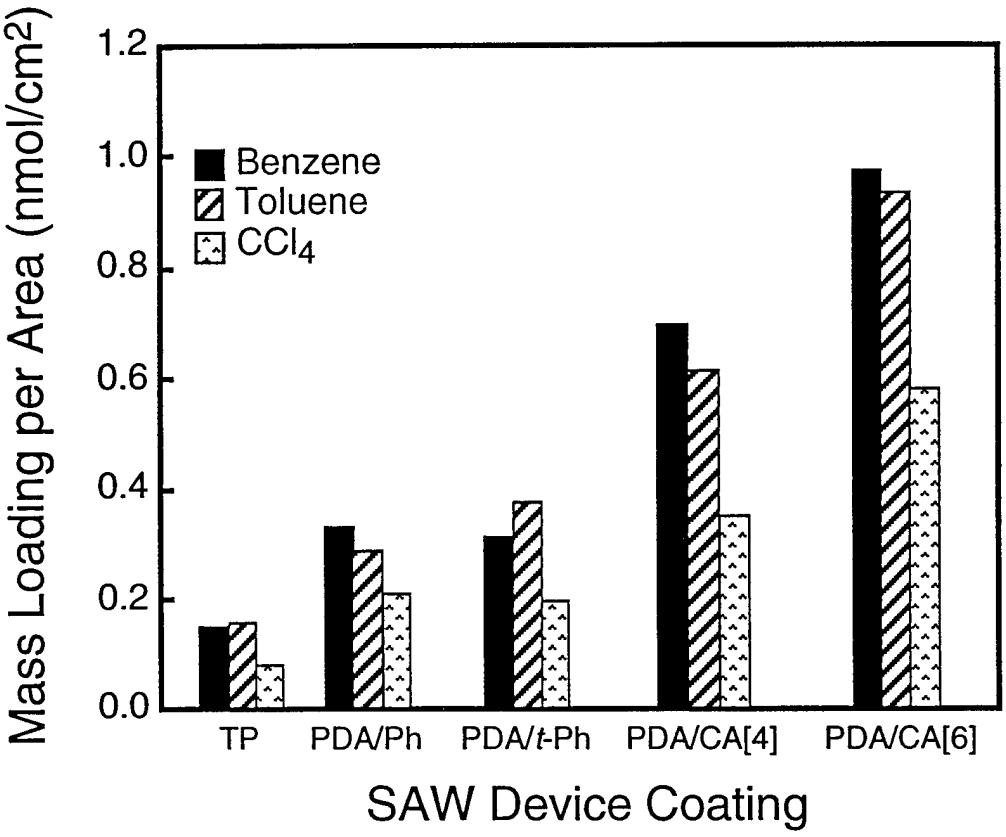

Figure 5/Crooks et al.

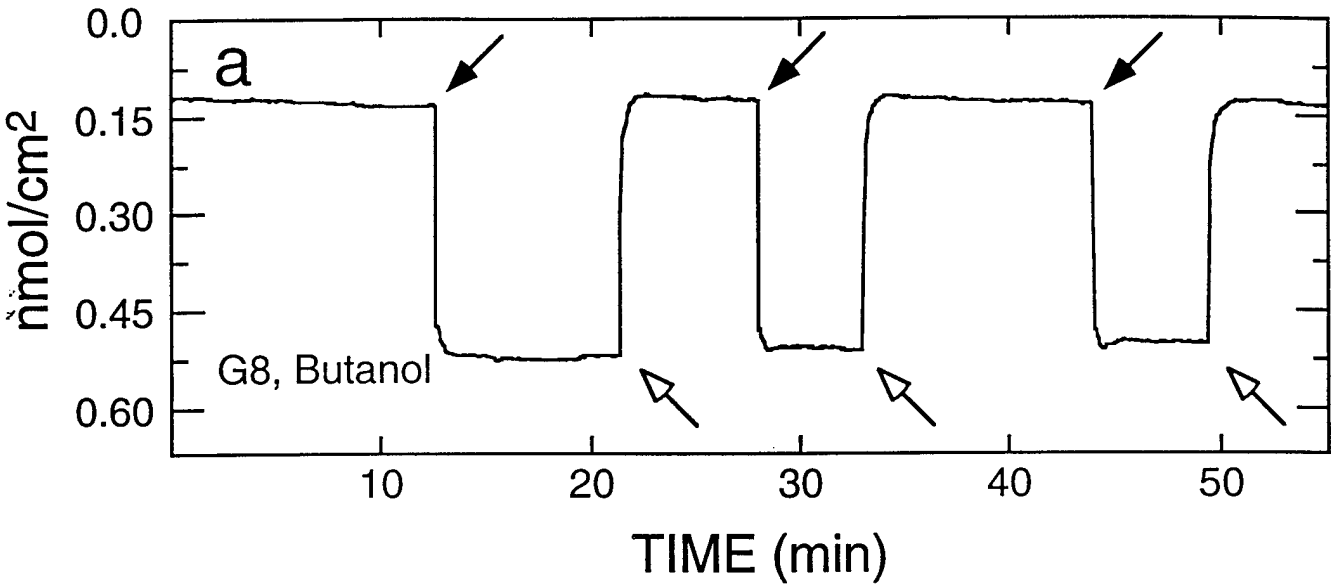

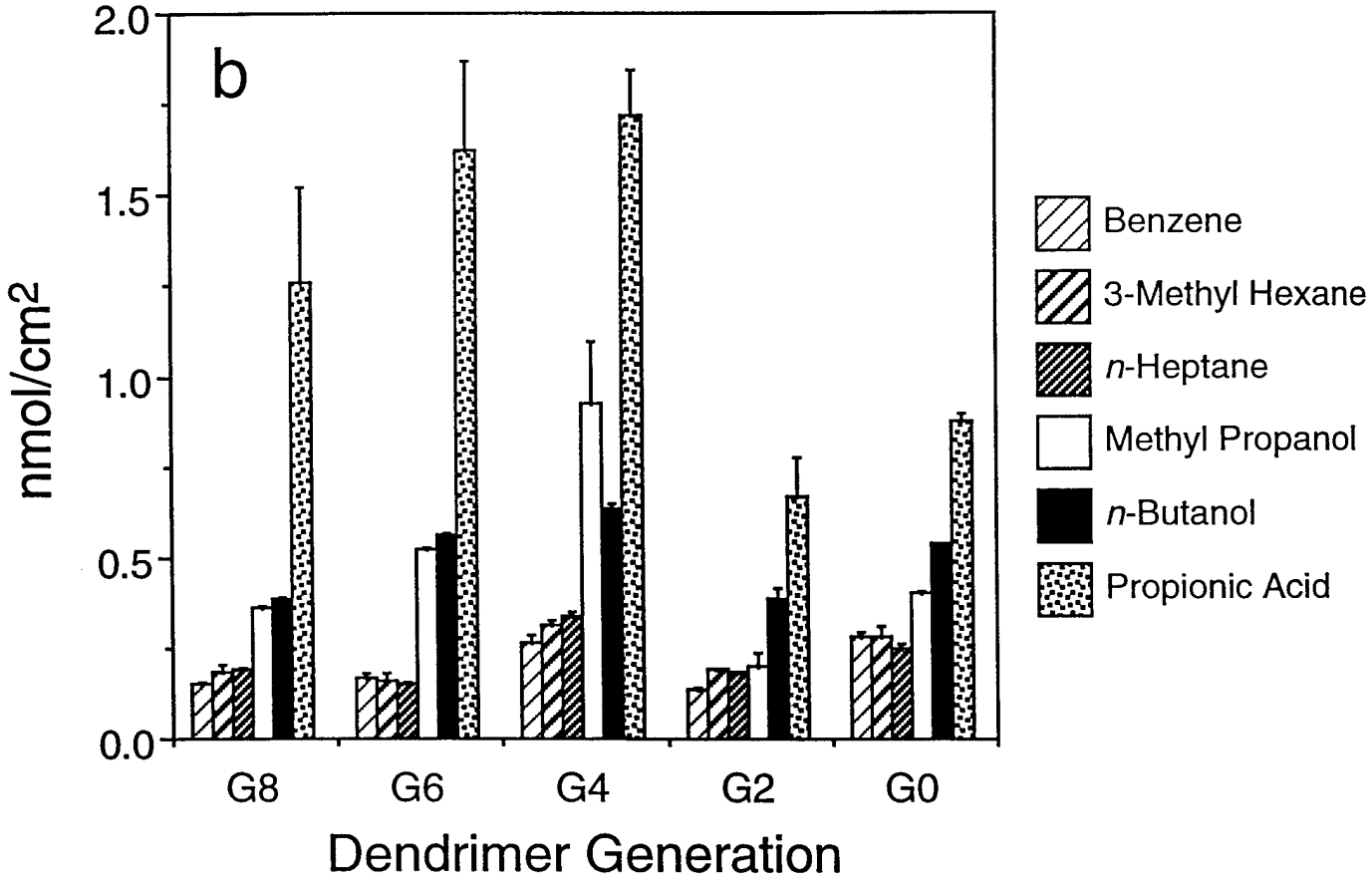

Figure 6/Crooks et al.